Applied Catalysis B: Environmental 312 (2022) 121407

Contents lists available at ScienceDirect

Applied Catalysis B: Environmental

journal homepage: www.elsevier.com/locate/apcatb

Cu and $CoFe_2O_4$ nanoparticles decorated hierarchical porous carbon: An excellent catalyst for reduction of nitroaromatics and microwave-assisted antibiotic degradation

Debika Gogoi [a], Rajeshvari Samatbhai Karmur [a], Manash R. Das [b,c], Narendra Nath Ghosh [a,*]

[a] Nano-Materials Lab, Department of Chemistry, Birla Institute of Technology and Science, Pilani K K Birla Goa Campus, Goa 403726, India
[b] Advanced Materials Group, Materials Sciences and Technology Division, CSIR-North East Institute of Science and Technology, Jorhat 785006, Assam, India
[c] Academy of Scientific and Innovative Research (AcSIR), Ghaziabad 201002, India

ARTICLE INFO

Keywords:
Cu
$CoFe_2O_4$ nanoparticles
Porous carbon
Reduction of aromatic nitrocompounds
Antibiotic degradation
Z-scheme catalyst
Microwave-assisted catalytic degradation

ABSTRACT

Water pollution is a major global issue that is causing tremendous threats to human health as well as to aquatic lives. This is triggering the need to develop efficient catalysts which can not only eliminate various water pollutants, but also cost-effective to use in a large-scale application. In this scenario, the biomass-derived porous carbon-supported catalyst which can catalyze multiple reactions to remove water pollutants is very much pertinent. Herein, we have synthesized a catalyst in which Cu and $CoFe_2O_4$ nanoparticles (CF) are anchored on the hierarchical porous carbon (PC) derived from coconut fibers. The catalytic efficiency of this catalyst (Cu-CF-PC) was tested for the removal of two major water pollutants, i.e. nitroaromatic compounds and antibiotics. Cu-CF-PC reduced various aromatic nitro compounds in presence of $NaBH_4$ within 0.5–3 min via a six electron transfer route. Furthermore, Cu-CF-PC also successfully degraded four commonly used antibiotics (Amoxicillin, Ciprofloxacin, Tetracycline hydrochloride, and Sulfamethoxazole) within 1 min. Degradation of antibiotics proceeds via a Z-scheme heterojunction formation in the catalyst under microwave irradiation which leads to the generation of $^{\bullet}OH$ radicals that degrades the antibiotic molecules. Moreover, the catalyst can be easily recovered from the reaction mixture by using an external magnet and reused. The catalyst was structurally and morphologically stable and showed ~92% catalytic efficiency even after five cycles. Hence, this work puts forward a reusable, cost-effective, environment-friendly, and highly efficient catalyst (Cu-CF-PC) that can be used in the practical approach to remediate environmental pollution.

1. Introduction

Water pollution is a major global environmental concern in today's scenario. With the advancement of human civilization, water bodies around the world are polluted by industrial wastes from varieties of industries, residues of pesticides, herbicides, different types of pharmaceutical pollutants, etc. [1–3] These pollutants are causing severe ecological damage to aquatic life and also posing great threats to human health. In this work, we are focusing on the removal of two types of pollutants: (i) nitroaromatic compounds, and (ii) different types of antibiotics (such as amoxicillin (AMX), ciprofloxacin (CPX), tetracycline hydrochloride (TCH), sulfamethoxazole (SMX), etc.).

Aromatic nitrocompounds are present in the wastewater released from different industries (such as paints, herbicides, pesticides, dyes and pigments, wood preservatives, refineries, etc.) [4,5]. The U.S. Environmental Protection Agency has categorized the aromatic nitrocompounds as very strong toxic pollutants to the ecosystem as these compounds are highly toxic in nature and harmful for humans as well as other living species [2,6]. Therefore, various strategies (e.g., electrolytic reduction, photocatalytic degradation, catalytic reduction, moist air oxidation, etc.) have been developed till date to remove these toxic nitroaromatic compounds from the industrial wastewater [7,8]. Among these methods, catalytic reduction of harmful nitroaromatic compounds to their respective aromatic amino products is a very advantageous method as the amino aromatic compounds are extensively used in the production of polymers, lubricants, analgesic drugs, agrochemicals, corrosion

* Corresponding author.
E-mail addresses: p20180429@goa.bits-pilani.ac.in (D. Gogoi), p20200051@goa.bits-pilani.ac.in (R.S. Karmur), mrdas@neist.res.in (M.R. Das), nghosh@goa.bits-pilani.ac.in (N.N. Ghosh).

https://doi.org/10.1016/j.apcatb.2022.121407
Received 29 January 2022; Received in revised form 25 March 2022; Accepted 10 April 2022
Available online 14 April 2022

inhibitors, etc. [5,9,10] The room temperature reduction of nitroaromatic compounds by $NaBH_4$ in aqueous medium is a very simple, highly efficient, economical, and eco-friendly method. Hence, there is an ongoing effort by researchers to develop efficient catalysts for this reaction.

Antibiotics are being used worldwide to treat and prevent various infectious diseases, to improve the growth rate and feed efficiency in animals. Antibiotics are also quite often used in agriculture and aquaculture [11–13]. Even today, in many places antibiotics are used in an unregulated manner. However, after administration a significant percentage of antibiotics are excreted into the environment [11]. In addition, the release of various pharmaceutical products from the industries as waste causes significant environmental pollution. These antibiotics retain in the environment for a long time and go through bioaccumulation and biomagnification which augments the antibiotic resistance bacteria or organisms and lateral gene transfer [14]. These genetically modified antibiotic-resistant organisms may create severe ecological impacts upon entering into the food chain and pose a great threat to human health. Hence, antibiotic resistance has been considered as a major global health crisis by the World Health Organisation (WHO) [15,16]. So in recent years, many physical, chemical, and biological approaches were developed for the efficient removal and decomposition of antibiotic residues. Among these, microwave (MW)-assisted catalytic degradation technique has gained a lot of attention as this technique shows high degradation efficiency, reduces the reaction time, enhances the reaction rate etc. In addition to its simple reaction conditions, microwave-based energies have advantages like high power generation, a good source of electrical energy, ease of generating and working with it, tunable energy delivery, etc. [17,18].

Therefore, in this present work, we have developed a multipurpose catalyst with Copper (Cu) and $CoFe_2O_4$ (CF) nanoparticles embedded within porous carbon (PC) matrix (Cu-CF-PC) to address the aforementioned issues. The Cu-CF-PC catalyst has been designed strategically so that each component can play important role in these two catalysis reactions. Here, Cu nanoparticles have been chosen so that they can act as catalytically active sites in the $–NO_2$ group reduction reaction by storing the electrons induced from BH_4, whereas in the microwave-assisted Cu-CF-PC catalyzed degradation of antibiotics Cu nanoparticles would play the role of an electron mediator between CF and PC which would enhance the catalytic efficiency of Cu-CF-PC. CF nanoparticles will induce a magnetic nature in the catalyst which would make the catalyst easily separable from reaction mixtures after completion of the reaction. Moreover, the MW absorption feature of CF will be helpful to generate high temperatures upon MW irradiation. The high surface area and porous structure of PC will provide strong solid support which could host CF and Cu nanoparticles and also assists during the catalytic reactions. Besides, the catalyst was synthesized from abundantly available coconut fiber-derived porous carbon and inexpensive, non-toxic chemicals which make the catalyst economically and environmentally favorable. To the best of our knowledge, a single catalyst that can show excellent catalytic efficiency towards reduction of various nitroaromatic compounds, as well as degradation of different antibiotics is not yet reported.

2. Experimental

2.1. Synthesis of the catalyst Cu-CF-PC

First, CF nanoparticles were synthesized by using a co-precipitation method and PC was synthesized from coconut fibers following the procedure reported in our previous works [19–21]. In the second step, CF-PC nanocomposite was synthesized by applying a wet-impregnation technique. Then, the synthesized CF-PC powder was soaked in the $CuCl_2.2H_2O$ solution for 6 h. 4 mL $NaBH_4$ solution was then added to the mixture dropwise and stirred for 3 h at room temperature. The product thus formed was washed with distilled water and dried at 60 °C for overnight. The yield of Cu-CF-PC was found to be ~99%. The synthetic route of Cu-CF-PC is briefly described in Scheme 1.

The details of the synthesis, characterization techniques, and instrumentation are given in the supplementary data.

2.2. Reduction of nitro compounds

In a 25 mL beaker, 4.5 mL of 9×10^{-2} mM solution of nitroaromatic compounds, and 1 mL of freshly prepared 0.2 M $NaBH_4$ solution were mixed and then 2.5 mL of the aqueous suspension of the catalyst (0.08 g L^{-1}) was added to this reaction mixture. 4 mL of the reaction mixture was immediately transferred to a quartz cuvette. The progress of the reaction was monitored by recording the absorbance spectra of the reaction mixture, using a UV–Visible (UV-Vis) spectrophotometer at a regular time interval, and LC-MS of the initial and final reaction mixture was recorded. After the completion of the reaction, the catalyst was magnetically separated from the reaction mixture, washed with distilled water, and then dried at 60 °C for further use.

2.3. Degradation of antibiotics

In a typical run, 7.5 mg catalyst was dispersed in 15 mL of the antibiotic solution (10 ppm in case of tetracycline hydrochloride (TCH), ciprofloxacin (CPX), sulfamethoxazole (SMX), and 50 ppm in case of amoxicillin (AMX)) taken in a 30 mL microwave reactor vessel. Then the reaction mixture was stirred in dark for 15 min to attain adsorption-desorption equilibrium. After the dark reaction, ~3 mL of the reaction mixture was extracted from the reaction mixture and its UV–Vis absorption spectra was recorded after separating the catalyst using an external magnet. This point was considered as the starting point (t = 0). Then, immediately 0.1 mL of H_2O_2 was added to the reaction mixture and it was exposed to microwave irradiation (250 W) in a microwave reactor for 1 min. The catalyst was separated from the reaction mixture and the absorption spectra was recorded after 1 min of microwave irradiation.LC-MS of the initial and final reaction mixture was recorded.

3. Result and discussion

3.1. Structure and morphology of the synthesized materials

Fig. 1a represents the XRD patterns of Cu-CF-PC which displays the characteristic peaks of CF nanoparticles at 2θ= 18.5°, 30.4°, 35.8°, 37.3°, 43.3°, 53.7°, 57.1°, 62.7° correspond to crystal planes (111), (220), (311), (222), (400), (422), (511), and (440), respectively (JCPDS card no. 22–1086) and metallic Cu at 2θ= 43.3°, 74.3° attributed to (111) and (220) diffraction planes (JCPDS card no. 04-0836) [19,22]. XRD patterns of pure CF and pure PC are shown in Fig. S1. The amorphous nature of pure PC was indicated by its XRD pattern which shows a broad hump centered at 2θ= ~23.2°. As a result of the poor diffraction intensity of PC, its XRD pattern was not visible in the XRD pattern of Cu-CF-PC [23]. The presence of PC in the Cu-CF-PC was identified from its Raman, FESEM, HRTEM, and EDX analysis. In the Raman spectrum of Cu-CF-PC, peaks at 282, 469, and 618 cm^{-1} are assigned to E_g, $T_{2\,g}$, and $A_{1\,g}$ modes of CF, and peaks at 1343 and 1594 cm^{-1} are assigned to the D and G bands of porous carbon which confirms the presence of CF and PC in the catalyst (Fig. 1b) [20,24]. The FT-IR analysis of the Cu-CF-PC also shows the presence of PC in it (Fig. S2).

FESEM and HRTEM analyses were used to investigate the microstructure of the catalyst (Cu-CF-PC). The 3-D porous structure of PC with a network of macropores and micropores are clearly visible in the FESEM micrograph of PC (Fig. 1c). Fig. 1d displays the FESEM image of the catalyst which reveals that the CF and Cu nanoparticles are distributed over the surface and inside the pores of PC. The HRTEM micrograph of the catalyst also confirms that the nanoparticles are dispersed in the carbon matrix (Fig. 2a). Fig. 2b features the lattice fringes corresponding to (111) plane of metallic Cu and (220), (311)

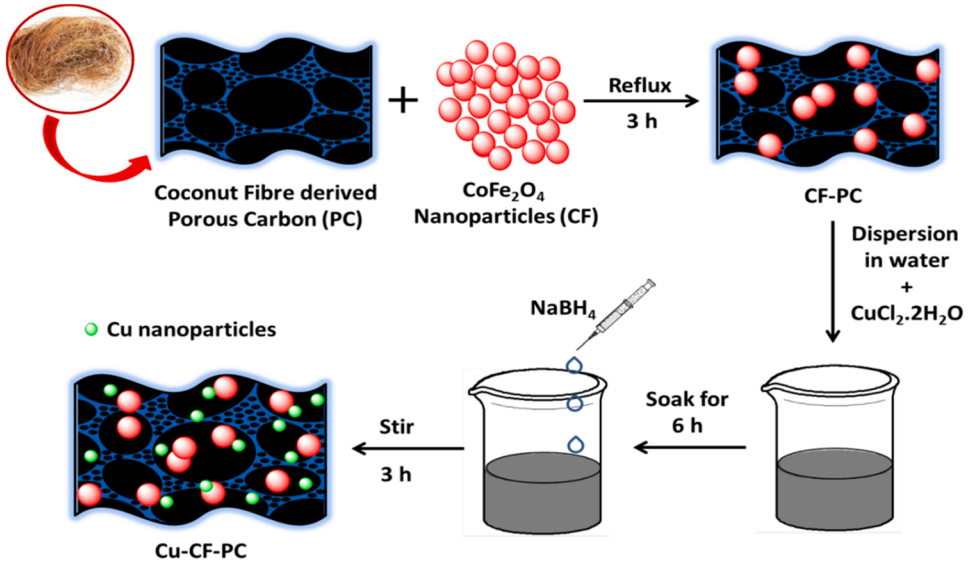

Scheme 1. Synthetic route of Cu-CF-PC nanocatalyst.

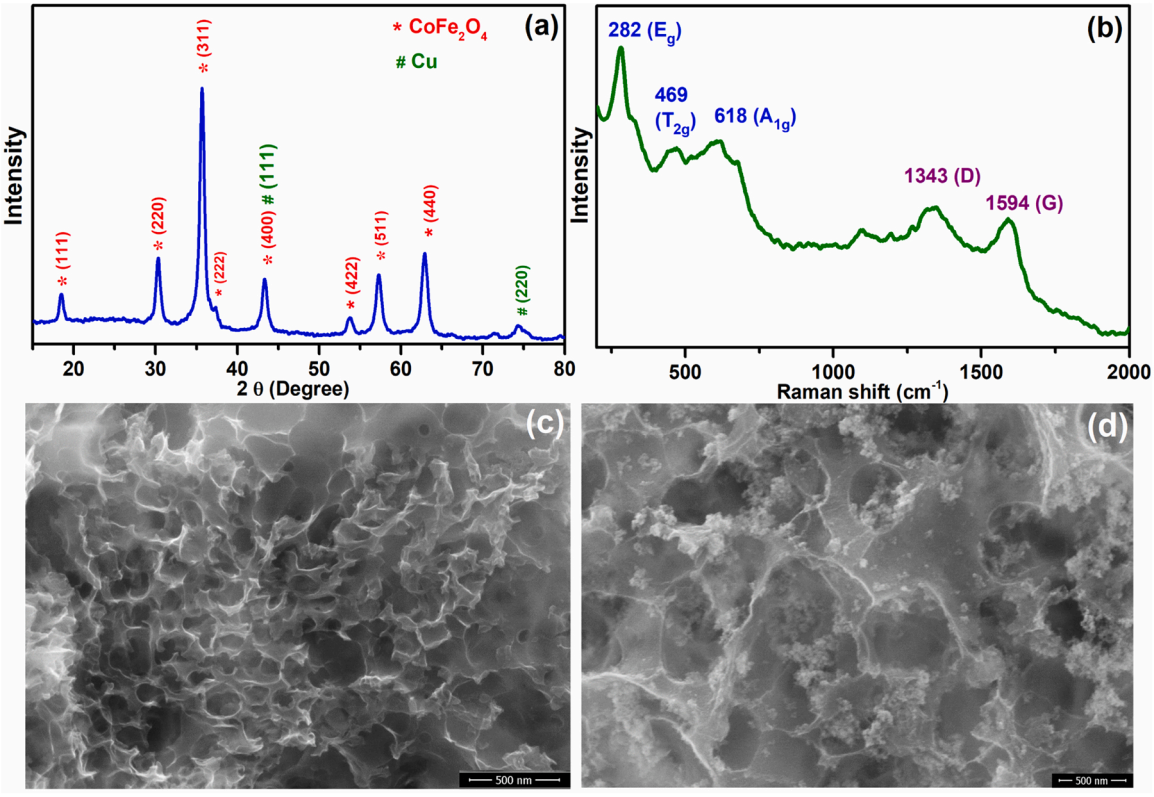

Fig. 1. (a) XRD pattern, (b) Raman spectrum of Cu-CF-PC, FESEM images of (c) pure porous carbon (PC), (d) Cu-CF-PC nanocatalyst.

planes of CF. Moreover, selected area electron diffraction (SAED) analysis of the catalyst showed its polycrystalline nature and exhibited Debye-Scherrer ring patterns for both $CoFe_2O_4$ and Cu nanoparticles as presented in Fig. 2c. Fig. S3 shows the EDX spectra of Cu-CF-PC which displays the characteristic peaks of C, O, Cu, Co, and Fe manifesting their presence in the catalyst. Besides, the elemental (EDX) mapping images of Cu-CF-PC (Fig. 2(d)) depict the spatial distribution of Fe, Co, C, O, and Cu in the catalyst which further confirms the presence of the above-mentioned elements in the catalyst.

The multiple-point BET surface area analysis of the materials was performed and the obtained N_2 adsorption-desorption isotherm of pure PC (Fig. S4a) and Cu-CF-PC (Fig. S4b) display the typical H3 hysteresis loop in a type-IV isotherm indicating the meso and macroporous nature of the materials [25]. The BET surface area, total pore volume, and pore surface area of pure PC were found to be ~1365 $m^2\ g^{-1}$, 0.41 $cm^3\ g^{-1,}$ and 531.9 $m^2\ g^{-1}$, respectively which was reduced to 434 $m^2\ g^{-1}$, 0.32 $cm^3\ g^{-1,}$ and 189.9 $m^2\ g^{-1}$ indicating the accommodation of CF and Cu nanoparticles in the porous surface of the PC.

The elemental compositions and their oxidation states in the Cu-CF-PC were analyzed by using XPS. In the XPS survey spectrum (Fig. S5) of

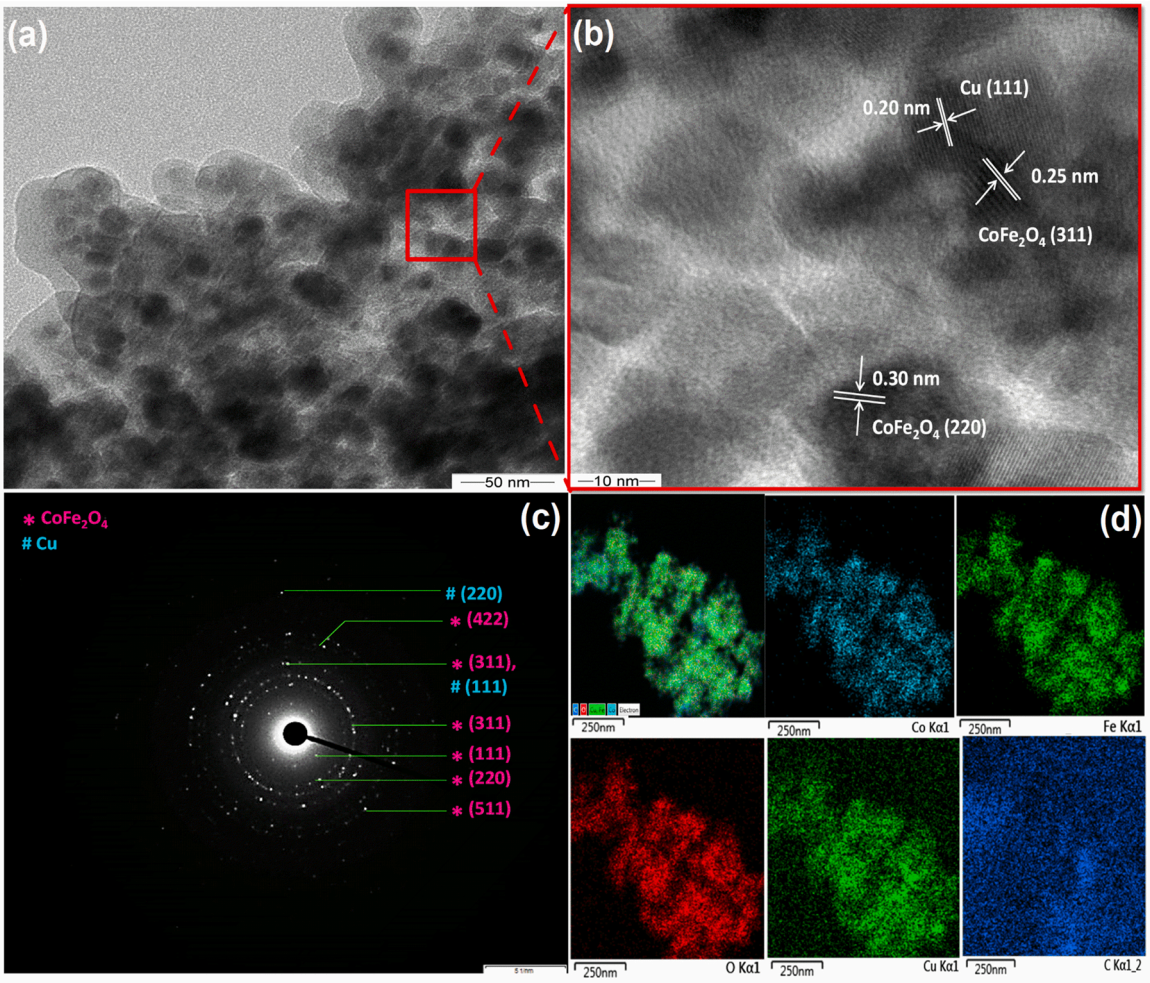

Fig. 2. (a) and (b) HRTEM images, (c) SAED pattern, (d) EDX mapping images of Cu-CF-PC nanocatalyst.

the Cu-CF-PC, all the peaks corresponding to C, O, Fe, Co, and Cu elements are observed which confirm their existence in the catalyst. Fig. 3a shows the high-resolution XPS spectrum of Co 2p, which is deconvoluted into two main peaks (781.3 eV and 797.1 eV) corresponding to the spin-orbit splitting of Co $2p_{3/2}$, Co $2p_{1/2}$, respectively, and their two shakeup satellite (sat) peaks (785.5 and 803.3 eV). This indicated the presence of Co^{2+} in the Cu-CF-PC [26,27]. The high-resolution Fe 2p spectrum (Fig. 3b) is fitted with four main peaks at 710.8, 713.6, 723.9, 726.4 eV, and two satellite peaks at 719.1, 732.62 eV. The Fe^{3+} present in the octahedral sites of CF generate the peaks at 711.3 (Fe $2p_{3/2}$), 724.8 eV (Fe $2p_{1/2}$), and Fe^{3+} present in the tetrahedral sites are liable for the peaks at 713.9 (Fe $2p_{3/2}$), 727.3 eV (Fe $2p_{1/2}$) [26,28]. Fig. 3c depicts the deconvoluted O 1 s spectrum, which is fitted with two peaks at 530.5 and 531.9 eV correspond to lattice oxygen bonding and oxygen-containing functional groups, respectively [26,29]. The deconvoluted Cu 2p spectrum is presented in Fig. 3d which shows peaks at 932.7 (Cu $2p_{3/2}$) and 952.8 eV (Cu $2p_{1/2}$) corresponding to Cu^0 [27,30]. The high-resolution XPS spectrum of C 1 s is presented in Fig. 3e in which three peaks at 284.6, 286.2, and 288.5 eV aroused due to the presence of C-C, C-O, and O-C═O, respectively, were observed [26,31].

The formation of Cu-CF-PC catalyst and the presence of Cu and CF nanoparticles within the porous structure of PC was confirmed from the XRD, Raman, FT-IR, FESEM, HRTEM, SAED, EDS, BET, and XPS analysis. Moreover, no changes in the structure of CF and the surface functional groups of PC occurred due to the addition of $NaBH_4$ during the catalyst synthesis.

3.2. Optical, electronic, and magnetic properties of the catalyst

The UV–Vis spectrum of Cu-CF-PC is presented in Fig. 4a which shows that the catalyst has a broad absorption range covering the entire UV–Vis spectrum range (200–800 nm) but the absorption intensity decreases in the UV region compared to that in the Visible light region. The bandgap energy (E_g) of pure CF and PC was found to be 1.04 and 1.42 eV, which was calculated from the Tauc's plot (Fig. S6) by using the Kubelka-Munk equation (Eq. (1)):

$$\alpha h\nu = A \quad (h\nu - E_g)^{n/2} \tag{1}$$

The band edge potential values of CB (E_{CB}) and VB (E_{VB}) in CF and PC was calculated by using Eqs. (2) and (3):

$$E_{CB} = \chi - E^e - \frac{1}{2}E_g \tag{2}$$

$$E_{VB} = E_{CB} + E_g \tag{3}$$

where E^e is the energy of free electrons in the material versus hydrogen i. e. 4.5 eV, and E_g is the bandgap energy. Electronegativity (χ) of the material was calculated by using the Eq. (4), in which x is the individual electronegativity value and a, b, c are the number of atoms of the elements A, B, and C, respectively, present in the compound [12,32].

$$\chi = [x(A)^a x(B)^b x(C)^c]^{1/(a+b+c)} \tag{4}$$

The calculated values of E_{CB} and E_{VB} are 0.8, 1.84 eV and 1.04, 2.46 eV, respectively, for pure CF and pure PC.

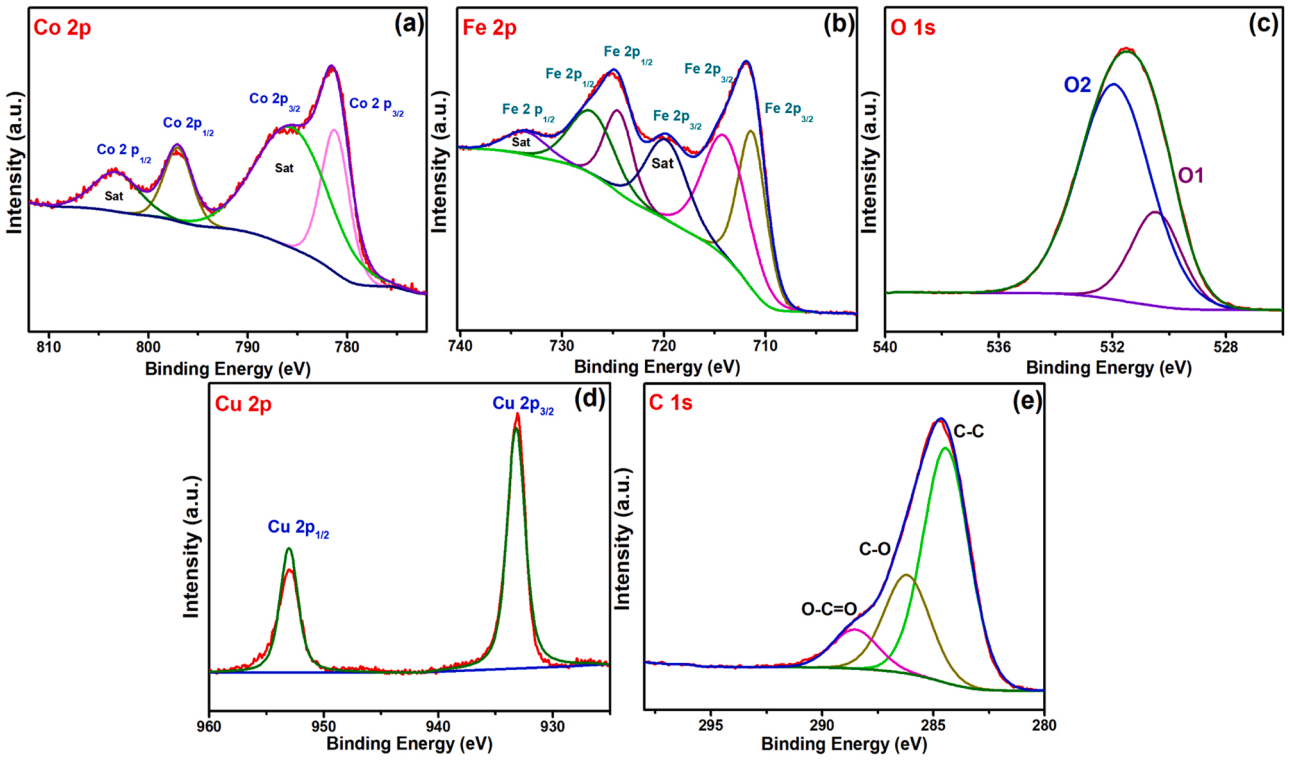

Fig. 3. The high resolution XPS spectra of (a) Co 2p, (b) Fe2p, (c) O 1s, (d) Cu 2p, and (e) C 1s.

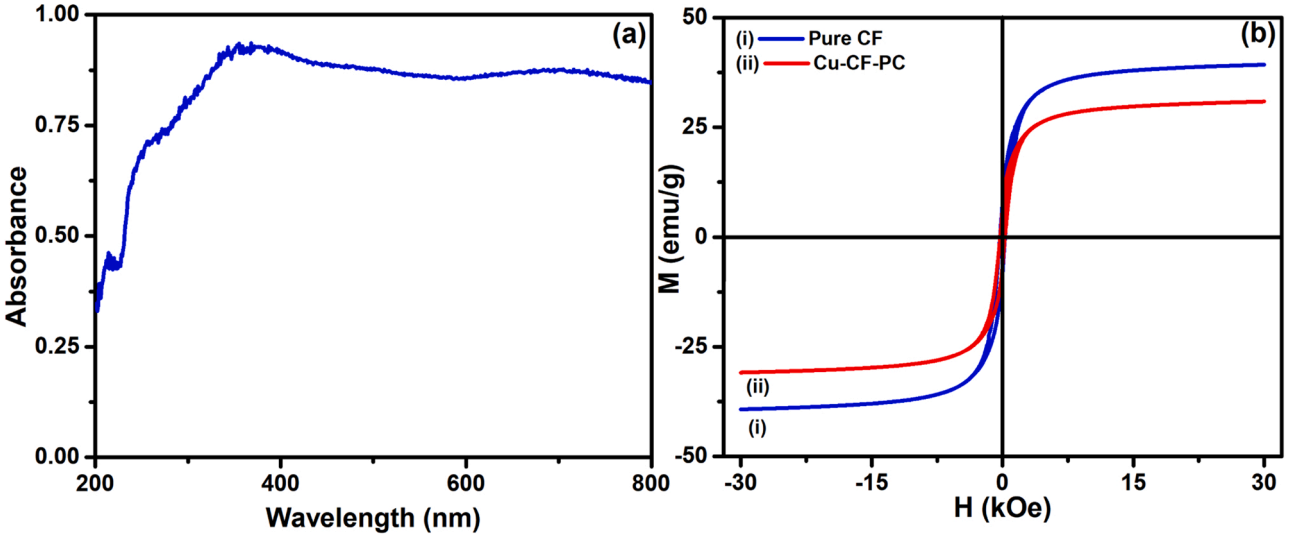

Fig. 4. (a) UV–Vis absorption spectra of Cu-CF-PC, (b) magnetic hysteresis loops of (i) pure CF, (ii) Cu-CF-PC at room temperature.

Magnetic properties of pure CF and Cu-CF-PC were analyzed by using a VSM and the hysteresis loop of both the materials recorded at room temperature is represented in Fig. 4b. In the case of pure CF, the saturation magnetization (M_s) and coercivity (H_c) values were found to be 39.3 emu g^{-1} and 296 Oe, respectively, which were decreased to 30.6 emu g^{-1} and 276 Oe in the case of Cu-CF-PC. This decrease of values might be due to the presence of Cu nanoparticles and PC matrix to CF in the nanocomposite. M_s value absolutely depends on the quantity of magnetic constituents present in the sample (Eq. (5)).

$$M_s = \Phi \times m_s \quad (5)$$

where, Φ is the fraction of volume, and m_s is the individual saturation magnetization of the magnetic constituents. Due to the incorporation of non-magnetic PC and diamagnetic Cu to CF nanoparticles, the M_s value of the nanocomposite became less than that of pure CF. H_c is a measure of the strength of the magnetic field that hinge on internal defects, crystallite size, anisotropy constant of materials, etc. Surface anisotropy of CF nanoparticles decreases when they are anchored in the carbon matrix and hence the H_c value of Cu-CF-PC is less than that of pure CF [33,34].

3.3. Reduction of nitro compounds

The catalytic activity of the synthesized Cu-CF-PC catalyst was estimated from the reduction reaction of a few aromatic nitro compounds to their respective amino products. First, the catalytic activity of Cu-CF-PC

was tested for the reduction reaction of 4-nitrophenol (4-NP) to 4-aminophenol (4-AP) in the presence of excess aqueous $NaBH_4$ at room temperature. This reduction reaction was also performed using pure CF and pure PC as catalysts. The progress of the reaction was monitored by using an UV–Vis spectrophotometer. The absorption maxima (λ_{max}) of the aqueous 4-NP solution was shifted from 317 nm to 400 nm after the addition of $NaBH_4$ due to the formation of phenolate ions and the color of the solution was turned to dark yellow from pale yellow [35]. It was observed that at least up to 30 min, no reduction reaction of 4-NP has occurred in absence of any catalyst and when pure PC was used as a catalyst. A negligible decrease in the absorbance of the mixture was observed when CF was used as a catalyst (Fig. 5a-c). The reaction was completed in 3, 6, and 2 min when pure Cu, CF-PC and Cu-PC were used as a catalyst, respectively (Fig. 5d-f). Whereas, in the case of Cu-CF-PC, 4-NP was reduced to 4-AP within 30 s. This indicated that in Cu-CF-PC nanocatalyst the active catalytic centers are provided mainly by Cu nanoparticles. The effect of mass loading of Cu nanoparticles in the catalyst on its catalytic performances is presented in Fig. S7. When the wt% of Cu nanoparticles was increased from 0% to 6%, the reaction completion time was reduced from 6 min to 30 s. The absorption peak at 400 nm was disappeared and a new peak at λ_{max}= 300 nm appeared which indicated the formation of 4-AP, as shown in Fig. 5g. From the obtained data, it can be concluded that Cu-CF-PC exhibited higher catalytic efficiency among all the synthesized materials, and hence it was

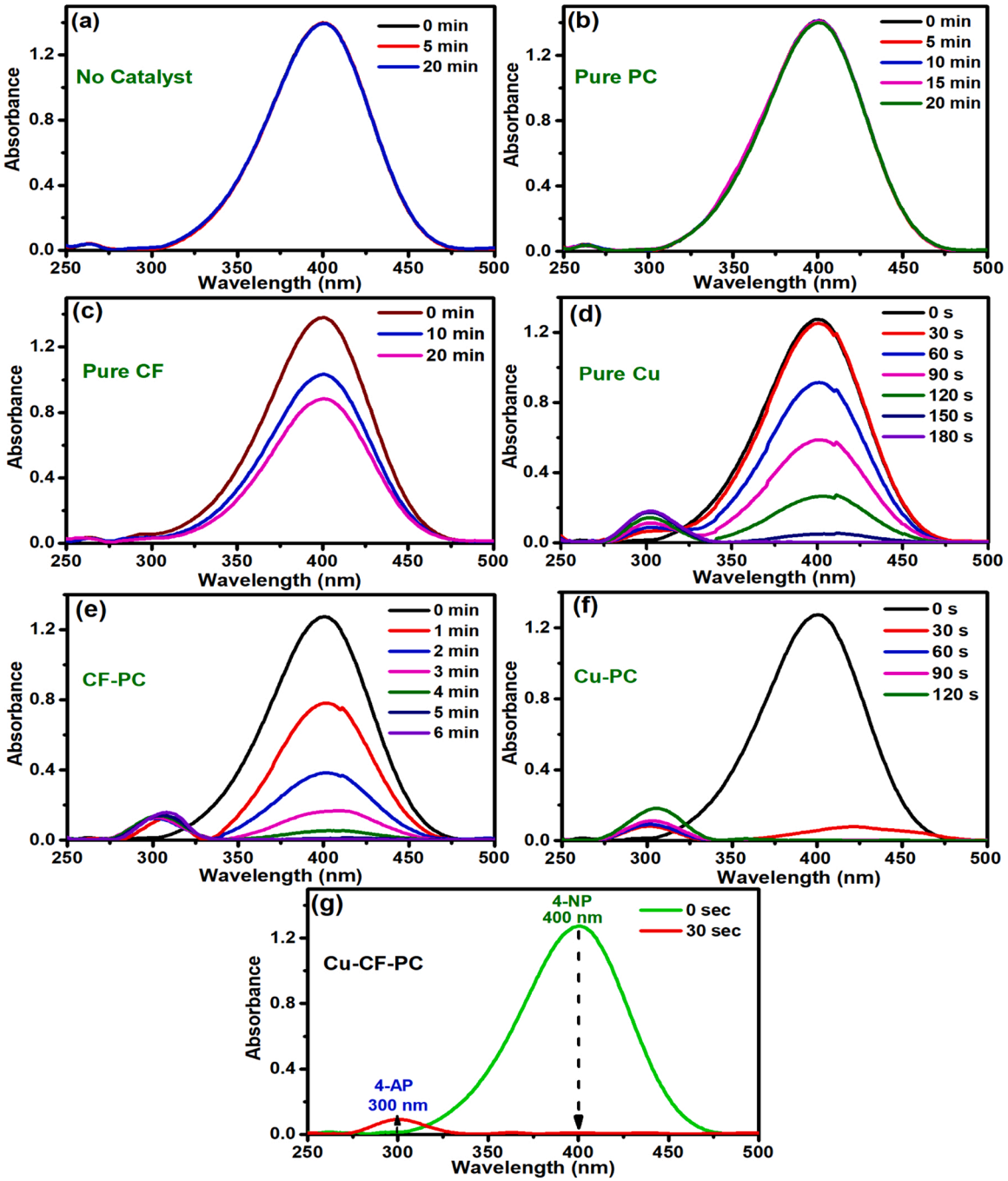

Fig. 5. Time-dependent UV–Vis spectra of the 4-NP reduction reaction when (a) no catalyst, (b) pure PC, (c) pure CF, and (d) pure Cu, (e) CF-PC, (f) Cu-PC, and (g) Cu-CF-PC were used. Reaction conditions: 4.5 mL of nitro aromatic compound (9×10^{-2} mM) + 1 mL $NaBH_4$ (0.2 M) + 2.5 mL aqueous suspension of the catalyst (0.08 g L^{-1}), aqueous medium, 25 °C.

used for the reduction of other nitroaromatic compounds.

The efficiency of the catalyst towards the reduction of each of the nitroaromatic compounds studied in this work is listed in Table 1 and the UV–Vis spectra are presented in Figs. 6 and S8. In the Figs. 5g, 6, and S8, it can be evidently noted that as the reaction proceeded, the peak intensity at the λ_{max} corresponding to the $–NO_2$ group of the compound was decreased and a new peak corresponding to their respective $–NH_2$ group of the products emerged which slowly increased to a certain intensity showing the gradual formation of the amino product. After the given time, the complete disappearance of the peak corresponding to $–NO_2$ group and no more increase in the intensity of the newly emerged peak corresponding to $–NH_2$ group, indicated the completion of the reduction reaction. The LCMS analysis of the reaction mixture before the reduction reaction and after the completion of the reaction also confirmed the formation of the amino products due to the Cu-CF-PC catalyzed reduction of nitroaromatic compounds (Figs. S9–S17), and ~100% conversion occurred within 30–180 s without the formation of any side-products. Moreover, no traces of unreacted starting nitroaromatic compound was detected that indicated ~ 100% theoretical yields and selectivity were achieved.

The reduction of nitroaromatic compounds in presence of aqueous

Table 1
The catalytic efficiency of Cu-CF-PC towards the reduction of various aromatic nitro compounds in presence of aqueous $NaBH_4$.

S. No.	Starting Material	Product	Reaction Completion Time (sec)	Conversion (%)
1	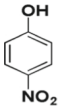	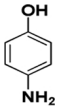	30	~100
2	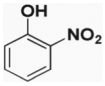	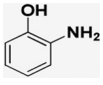	30	~100
3	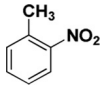	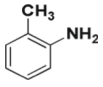	90	~100
4	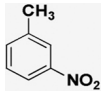	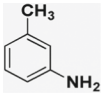	90	~100
5			60	~100
6	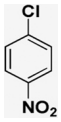	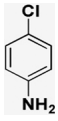	180	~100
7	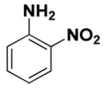	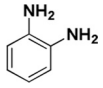	30	~100
8	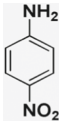	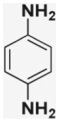	30	~100
9	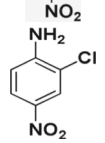	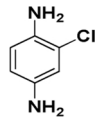	30	~100

Reaction conditions: 4.5 mL of nitro aromatic compound (9×10^{-2} mM) + 1 mL $NaBH_4$ (0.2 M) + 2.5 mL aqueous suspension of the catalyst (0.08 g L^{-1}), aqueous medium, 25 °C.

$NaBH_4$ follows an electron transfer (ET)-induced hydrogenation mechanism that includes six electron transfer processes. At the initial stage of the reaction, BH_4^- ions get adsorbed on the surface of the catalyst, and then the generation of active hydrogen atoms occurs ensue from the transfer of electrons channeling from BH_4^- to the active sites (Cu nanoparticles) of the catalyst [5,22]. These active hydrogen species reduce the $–NO_2$ group to $–NH_2$ group and the plausible mechanism is illustrated in Scheme 2. For instance, the reduction of 4-NP to 4-AP proceeds as 4-nitrophenol → 4-nitrosophenol → 4-hydroxyaminophenol → 4-aminophenol [36].

The preeminent catalytic activity of Cu-CF-PC can be explained from the following points: (i) Cu nanoparticles store the electrons after ET from BH_4^- and acts as the main catalytic active sites of Cu-CF-PC, (ii) the presence of CF makes the catalyst magnetic in nature and easily separable from the reaction mixture, (iii) the presence of PC assists to enhance the catalytic activity of the catalyst as it provides more surface area for adsorption of the reactants followed by the diffusion of the reactants into catalytically active sites. Thus the probability of contact of the reactant molecules with the active sites increases and subsequently rate of reduction also increases. PC also facilitates electron transport to the reactant by channeling them through its porous network. Besides, the agglomerations of the active sites are prevented as they are distributed throughout the carbon matrix of PC [37,38]. (iv) a synergistic effect arises from the hierarchical structure of the nanocatalyst, where Cu and CF nanoparticles are embedded within the porous structure of PC. This factor plays an important role in the excellent catalytic activity of Cu-CF-PC. The catalytic efficiency of Cu-CF-PC was found to be remarkably higher in comparison to some of the already reported catalysts in the reduction of nitroaromatic compounds in presence of aqueous $NaBH_4$ (Table S1).

The excellent catalytic efficiency of Cu-CF-PC was also advantageous in the reduction of the toxic herbicide trifluralin, which contains two $–NO_2$ groups. It has been observed that Cu-CF-PC has the potentiality to reduce this toxic nitroaromatic compound in presence of $NaBH_4$ within 25 min (Fig. S18).

3.3.1. *Effect of inorganic anions in the catalytic reduction of nitroaromatic compounds*

The reduction of 4-NP was carried out in the presence of various inorganic anions (Cl^-, NO_3^-, HCO_3^-, and SO_4^{2-}) having a concentration of 0.1 M, in order to investigate the effect of the presence of these anions on the catalytic efficiency of Cu-CF-PC. The presence of these anions hindered the reduction of 4-NP in the order $SO_4^{2-} > HCO_3^- > NO_3^- > Cl^-$ (Fig. S19). This could be explained as due to the weaker electrostatic repulsion force between the catalyst surface and anions with large size or high valence state, these anions exist in the vicinity of the catalyst surface. Hence, these anions hinder the adsorption of the reactants on the surface of the catalyst and subsequently reduce the catalytic activity of the catalyst [39,40].

3.4. *Microwave-assisted catalytic degradation of antibiotics*

The catalytic efficiency of Cu-CF-PC towards the degradation of antibiotics was determined from the microwave-assisted degradation of a few commonly used antibiotics such as amoxicillin (AMX), ciprofloxacin (CPX), tetracycline hydrochloride (TCH), and sulfamethoxazole (SMX), in the presence of H_2O_2. Fig. S20a shows that the % degradation of CPX (10 ppm) rose from ~90 to ~100% when the catalyst dose was increased from 0.1 to 0.5 g L^{-1} after only 1 min of microwave irradiation. No degradation of the antibiotic was observed in absence of the catalyst or microwave irradiation. To understand the role of H_2O_2, the reactions were carried out in the presence of only catalyst (without H_2O_2), only H_2O_2 (without catalyst), and in presence of both catalyst and H_2O_2. The catalyst (Cu-CF-PC) has degraded ~85% of CPX within 1 min in absence of H_2O_2. Whereas, when only H_2O_2 was present, nearly 12% of CPX was degraded in 1 min ~100% degradation was observed in

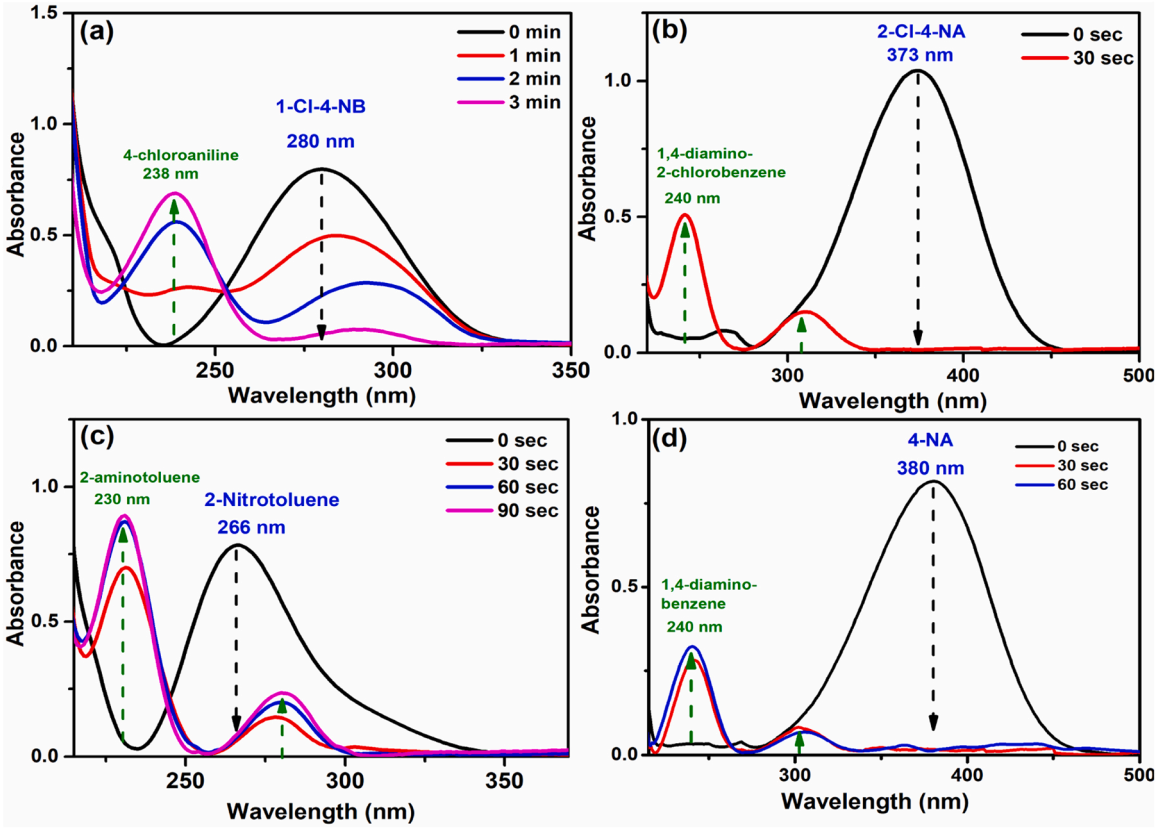

Fig. 6. Time-dependent UV–Vis spectra of Cu-CF-PC catalyzed reduction reaction of (a) 1-chloro-4-nitrobenzene (1-Cl-4-NB), (b) 2-chloro-4-nitroaniline (2-Cl-4-NA), (c) 2-nitrotoluene, and (d) 4-nitroaniline. Reaction conditions: 4.5 mL of nitro aromatic compound (9×10^{-2} mM) + 1 mL $NaBH_4$ (0.2 M) + 2.5 mL aqueous suspension of the catalyst (0.08 g L^{-1}), aqueous medium, 25 °C.

presence of both (Cu-CF-PC and H_2O_2) in 1 min (Fig. S20b). Thus, it was concluded that in this Cu-CF-PC catalyzed reaction, H_2O_2 acts as a sacrificial agent by generating $^{\bullet}OH$ radicals under microwave irradiation. Fig. 7 displays that, in the UV–Vis spectra of AMX, TCH, CPX, and SMX the maximum absorbance peak (λ_{max}) at 231, 360, 272, and 265 nm, respectively, disappears after 1 min of microwave irradiation in presence of H_2O_2. The complete degradation of the antibiotics in this reaction was also confirmed from the LCMS analysis of the antibiotic solutions before and after microwave irradiation and the obtained data are presented in Figs. S21–S24. The total organic carbon (TOC) of the antibiotics were analyzed before and after the degradation reactions and the obtained data are presented in Table S2. The TOC removal ratio was calculated by using Eq. (6) [19]:

$$\frac{TOC_i - TOC_f}{TOC_i} \tag{6}$$

where TOC_i and TOC_f are the obtained TOC contents of the antibiotic solutions before and after the degradation reactions. For TCH, CPX, AMX, and SMX, the TOC removal ratios were found to be 79.07%, 71.46%, 78.40%, and 75.67%, respectively.

3.4.1. *Plausible reaction mechanism*

The present study clearly demonstrates that Cu-CF-PC nanocatalyst acts highly efficient manner toward the MW-assisted catalytic degradation of various antibiotics in the aqueous medium. Each component of this catalyst (such as Cu nanoparticles, CF, and PC) plays an important role. Our previous study demonstrated that $CoFe_2O_4$ possesses significantly high MW absorption property due to its excellent real and imaginary permittivity and permeability values [41]. This characteristic of CF we have exploited to design the present catalyst, so that CF nanoparticles can be helpful to generate high temperature within the catalyst during MW irradiation. The magnetic nature of CF would help to focus the EM wave within the reactor [41]. Owing to the possession of the high surface area and porous structure, PC accommodates CF and Cu nanoparticles and acts as a support matrix. Its porous structure helps to absorb the antibiotic molecules within the catalysts and provides a shorter transportation path to the catalytically active sites. Moreover, several authors have reported that the strong interactions between MW and carbon materials generate hot spots which accelerate the reaction rate [42–44].

The role of Cu, CF, and PC in the catalytic activity of Cu-CF-PC towards the degradation of antibiotics was determined by using pure CF, pure PC, pure Cu, CF-PC, and Cu-PC as the catalyst in the degradation reaction of CPX (Fig. S25). After 1 min of MW irradiation and in the presence of H_2O_2, the % of degradation of CPX was found to be ~49, ~63, and ~65% when pure CF and PC, and Cu-PC were used as the catalyst, respectively. Whereas CF-PC degrades ~86% and pure Cu nanoparticles degrade ~15% of CPX which is almost equivalent to the % of degradation of CPX when only H_2O_2 was present. But when Cu was incorporated into CF-PC, ~100% degradation occurred in 1 min. This indicated that pure Cu nanoparticles cannot degrade the antibiotic molecules itself but enhances the catalytic performance of CF-PC.

When antibiotic molecules adsorbed on the surface of Cu-CF-PC catalyst are exposed to MW irradiation, a high temperature is attained in the hot spots. Under this condition, CF (bandgap = 1.04 eV) and PC (bandgap = 1.42 eV) get excited and generate electrons and holes. Then, the electron transfer occurs from CB of PC (1.04 eV) to VB of CF (1.84 eV), and Cu nanoparticle, sandwiched between CF and PC acts as an electron mediator to promote this electron transfer, and also prevents the recombination of holes and electrons in CF and PC [45,46]. Thus the useless electrons and holes recombine, the powerful hole and electrons generated at the CB of CF (0.84 eV) and VB of PC (2.46 eV) produce

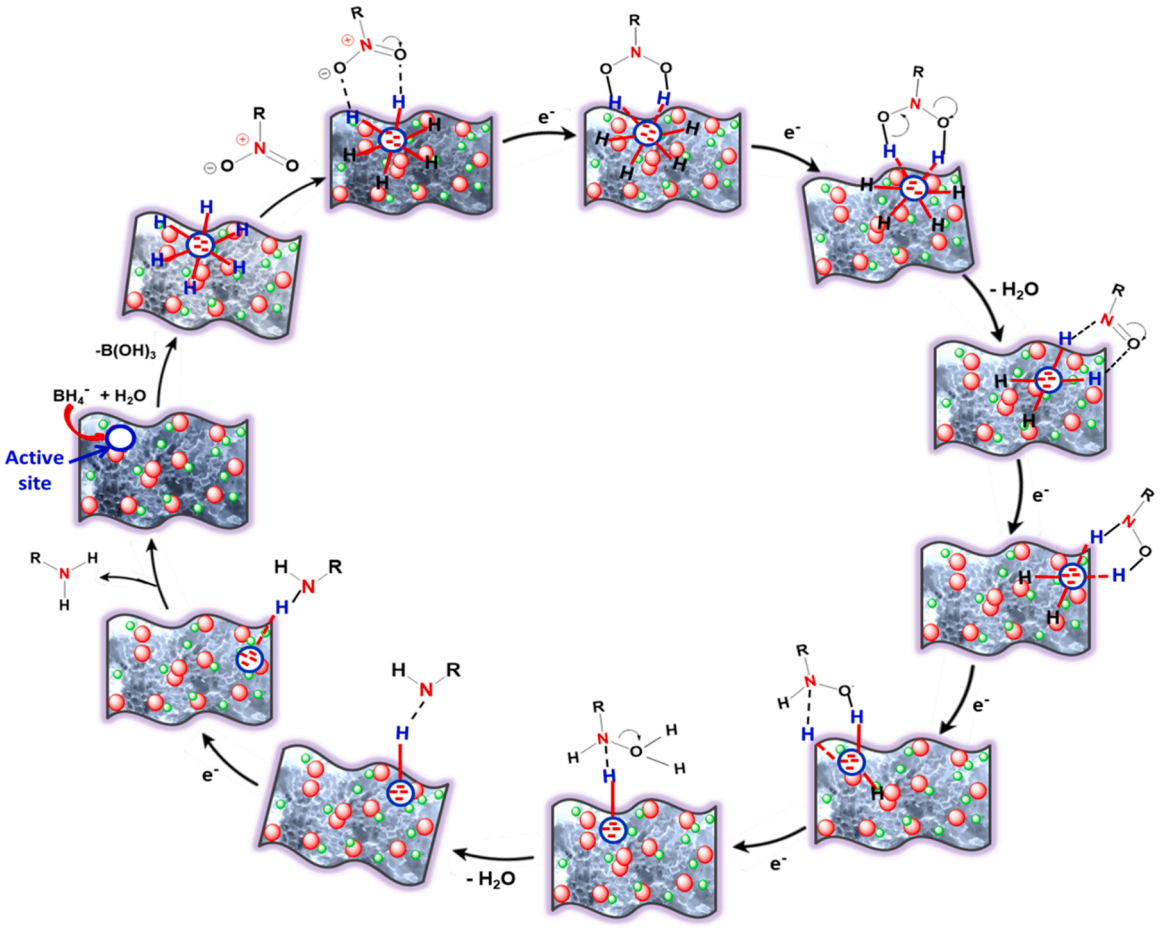

Scheme 2. The plausible mechanism involved in the room temperature reduction of aromatic nitro compounds by Cu-CF-PC, in the presence of $NaBH_4$.

radicals ($^{\bullet}OH$) by reacting with H_2O and sacrificial agent H_2O_2. The plausible reactions, which are involved in the generations of $^{\bullet}OH$ radicals by the Cu-CF-PC nanocatalyst under microwave irradiation are presented in Eqs. (7) and (8) [47,48]:

$$H_2O + h^+ \rightarrow {}^{\bullet}OH + H^+ \ (1.14\ V) \quad (7)$$

$$H_2O_2 + H^+ + e^- \rightarrow H_2O + {}^{\bullet}OH \ (2.32\ V) \quad (8)$$

The Z scheme mechanism which is involved in this process is depicted in Scheme 3. Thus, the generated $^{\bullet}OH$ radicals attack the antibiotic molecules to degrade them to small molecules and mineral substances (H_2O, CO_2, etc.) To understand the role of $^{\bullet}OH$, h^+, and e^- in the reaction mechanism, the degradation reaction of SMX was carried out in the presence of isopropyl alcohol (IPA) (as $^{\bullet}OH$ scavenger), methanol (as h^+ scavenger), and dimethyl sulfoxide (DMSO) (as e^- scavenger) (Fig. S26) [19,39]. After 1 min of MW irradiation, the degradation % of SMX was reduced to ~46, ~61, and ~83% in presence of IPA, methanol, and DMSO, respectively. This indicated the formation of $^{\bullet}OH$, h^+, and e^- due to the MW irradiation and their participation in the reaction mechanism. The $^{\bullet}OH$ radicals play a major role in the degradation of the antibiotics which is also supported by other substantive findings in the literature [3,12,14,17,49–53].

The enhanced charge transfer phenomena in Cu-CF-PC compared to that of pure CF and PC can also be explained from the electrochemical impedance spectroscopy (EIS) measurements. The charge transfer resistance (R_{CT}) values of Cu-CF-PC was found to be 0.51 Ω, which is much lower than that of pure CF (13.8 Ω) and PC (2.29 Ω) [21]. Fig. 8a shows the Nyquist plot of the materials. In the frequency vs. phase angle plot (Fig. 8b), it was observed that Cu-CF-PC showed the highest capacitive behavior with a phase angle 80° at the lower frequency region, and the relaxation time ($\tau o = f_o^{-1}$) of Cu-CF-PC was decreased to 3.41×10^{-3} s. Whereas, phase angles and τo values of pure CF and pure PC were 71°, 67° and 0.072, 2.5 s respectively [21]. Therefore, the presence of Cu promotes the charge transfer in the catalyst via Z-scheme heterojunction and extends the lifetime of the microwave-induced powerful charge carriers which generates the active radicals and degrades the antibiotics. Furthermore, from the comparative study, it was observed that the catalytic efficiency of Cu-CF-PC to degrade various antibiotics was far more superior as compared to some of the already reported catalysts (Table S3).

As a representative, the plausible degradation pathway of AMX is presented in Scheme 4. LC-MS analysis (Fig. S21b) identifies some of the intermediates and degraded molecules. AMX ($m/z = 366$) undergoes $^{\bullet}OH$ attack to form I-2 ($m/z = 431$), which is due to the cleavage of four C—H bonds followed by attachment of four hydroxyl groups in these positions. I-2 further decomposes into I-7, I-8, I-13 after C—C and C—N bond breaking due to $^{\bullet}OH$ attack and I-3 forms due to decarboxylation. Hydration of AMX produces I-1 which can be decarboxylated to form I-6 and C—N bond cleavage of I-6 give I-11 and I-12. Further $^{\bullet}OH$ attack on I-12 gives I-16 and I-11 decomposes to produce I-17 and I-18 via intermediates I-15 and I-19. Another possible degradation pathway of AMX is through C—N bond cleavage due to hydration to form I-4 and I-5 which undergoes decarboxylation upon $^{\bullet}OH$ attack to produce I-9 and I-10. I-9 decomposes to I-14 followed by ring cleavage to form I-17 and I-18.

The possible MW-assisted degradation pathways for other antibiotics (CPX, TCH, and SMX) based on the corresponding LCMS spectra (before and after the reaction) are presented in the supplementary data

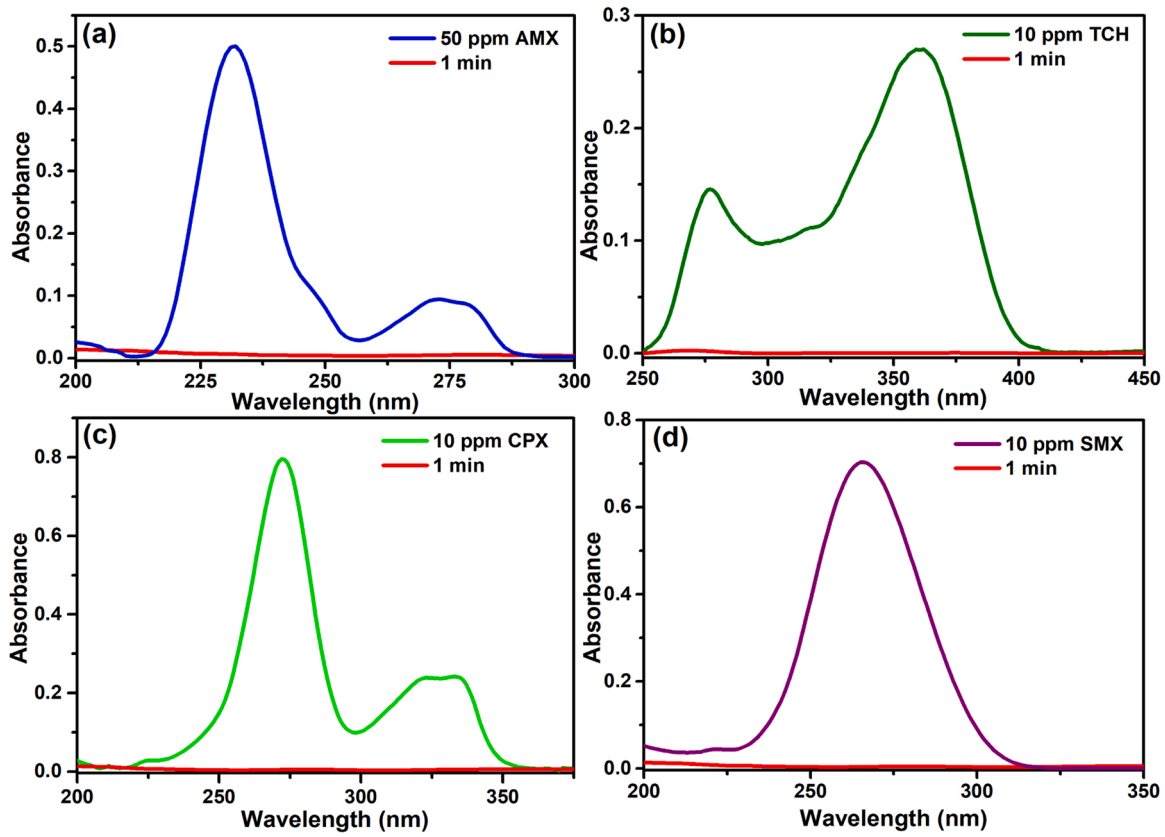

Fig. 7. Degradation of (a) AMX, (b) TCH, (c) CPX, and (d) SMX by Cu-CF-PC in presence of H_2O_2 monitored by UV–Vis spectroscopy. Reaction conditions: 15 mL of antibiotic solution (10 ppm) + 0.1 mL H_2O_2 (30%) + catalyst (0.5 g L^{-1}), 120 °C, MW power = 250 W.

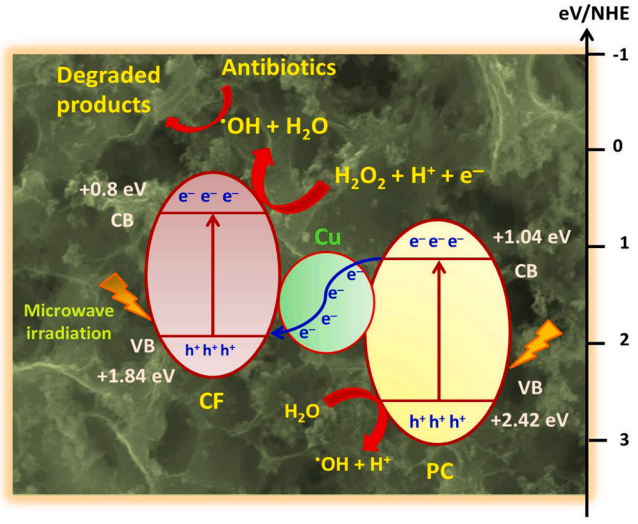

Scheme 3. MW-assisted degradation of antibiotics by Cu-CF-PC via a Z-scheme mechanism.

(Schemes S1–S3).

3.4.2. *Effect of inorganic anions in the degradation of antibiotics*

The effect of the presence of inorganic anions on the degradation of antibiotics was studied by performing the degradation reaction of SMX in the presence of some commonly existing anions such as Cl^-, NO_3^-, HCO_3^-, and SO_4^{2-} (0.1 M) in the reaction mixture. It was observed that the % of degradation was reduced to ~72, ~81, ~87, and ~89% when Cl^-, HCO_3^-, NO_3^-, and SO_4^{2-} were present, respectively (Fig. 9). This might be due to the fact that these anions are acting as $^{\bullet}OH$, h^+, and e^- scavengers by reacting with these species as represented in Eqs. (9)–(17) [54–57].

$$Cl^- + h^+ \rightarrow Cl^{\bullet} \quad (9)$$

$$Cl^- + {}^{\bullet}OH \rightarrow {}^{\bullet}ClOH^- \quad (10)$$

$$Cl^- + Cl^{\bullet} \rightarrow {}^{\bullet}Cl_2^- \quad (11)$$

$$HCO_3^- + {}^{\bullet}OH \rightarrow CO_3^{\bullet -} + H_2O \quad (12)$$

$$NO_3^- + h^+ \rightarrow NO_3^{\bullet} \quad (13)$$

$$NO_3^- + {}^{\bullet}OH \rightarrow NO_3^{\bullet} + OH^- \quad (14)$$

$$SO_4^{2-} + h^+ \rightarrow SO_4^{\bullet -} \quad (15)$$

$$SO_4^{2-} + {}^{\bullet}OH \rightarrow SO_4^{\bullet -} + OH^- \quad (16)$$

$$SO_4^{\bullet -} + e^- \rightarrow SO_4^{2-} \quad (17)$$

These produced species are less reactive as compared to $^{\bullet}OH$ and because of this, the degradation of SMX was reduced in the presence of these inorganic anions.

3.5. *Catalyst reusability and stability*

After the completion of the reactions, the catalyst was separated from the reaction mixture by using a NdFeB (N-35 grade) magnet with BH_{max}= 33–36 MGOe. Then the catalyst was washed with distilled water followed by ethanol and then dried at 60 °C for further use. After the recovery of the catalyst, atomic absorption spectroscopy (AAS) analysis of the reaction mixture was carried out and no significant amount of metal leaching from the Cu-CF-PC had been observed during the catalysis reactions. The reusability of the catalyst was tested for five cycles and it was observed that after the first three cycles the efficiency

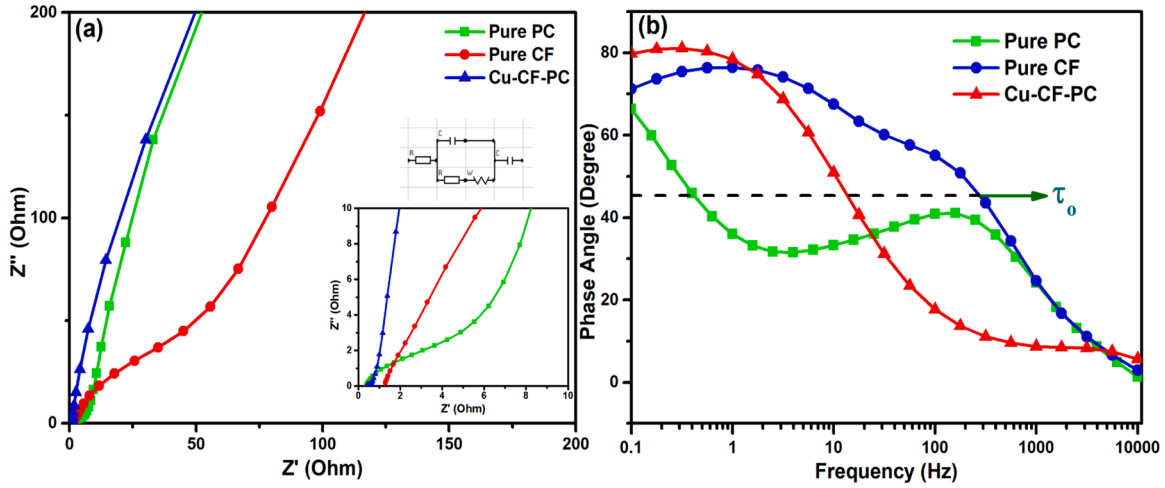

Fig. 8. (a) Nyquist plot, (inset: EIS values at the low-frequency region, and equivalent circuit used for fitting the data), (b) Bode plot (phase angle vs. frequency) of pure PC, pure CF, Cu-CF-PC.

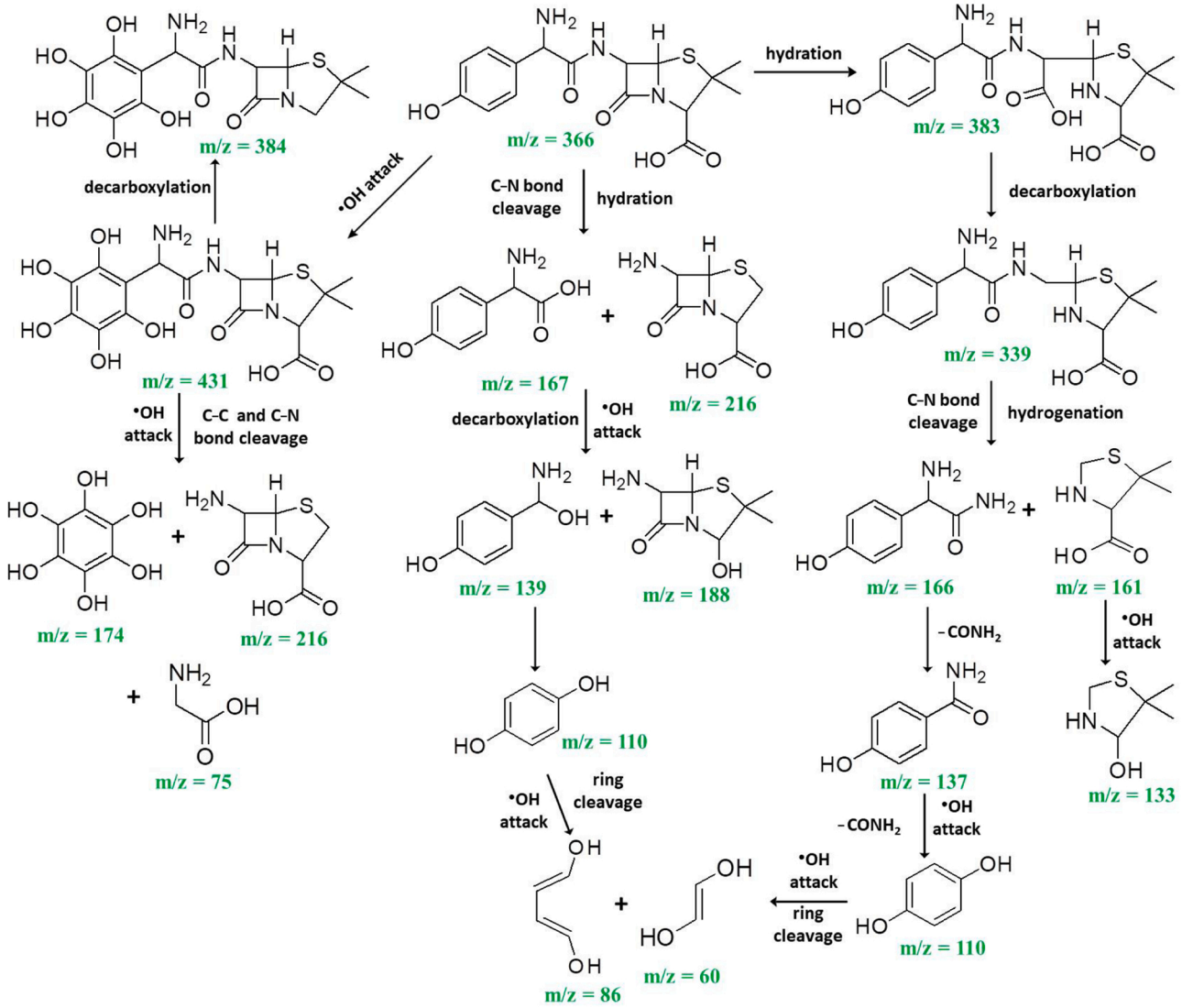

Scheme 4. The plausible degradation pathways of AMX by Cu-CF-PC under MW irradiation based on the LC-MS analysis data of AMX after degradation.

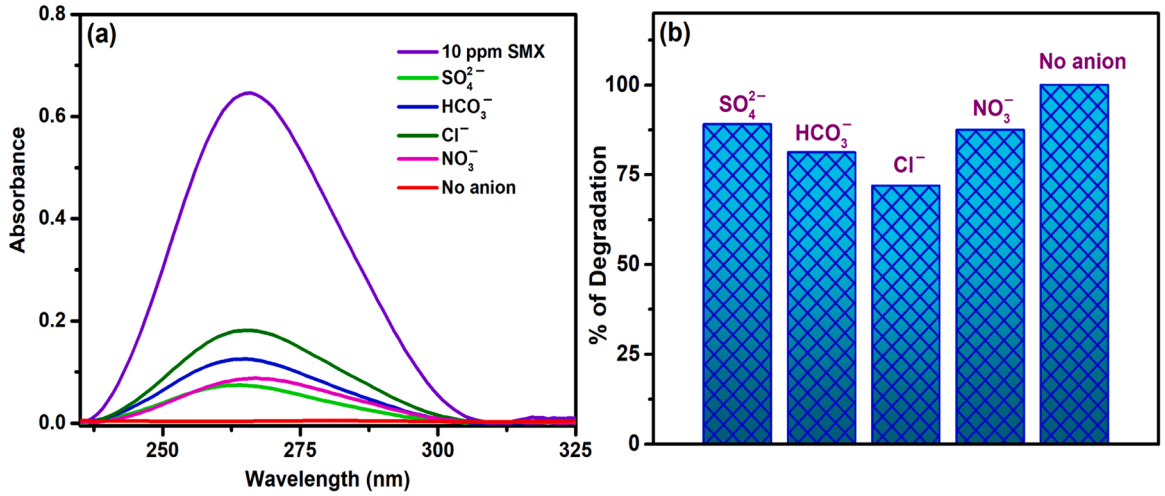

Fig. 9. (a) Obtained UV–Vis spectra, and (b) % of degradation of SMX after 1 min of MW irradiation in the presence of various inorganic anions. Reaction conditions: 15 mL of antibiotic solution (10 ppm) + 0.1 mL H_2O_2 (30%) + catalyst (0.5 g L^{-1}) + 0.1 M inorganic anions, 120 °C, MW power = 250 W.

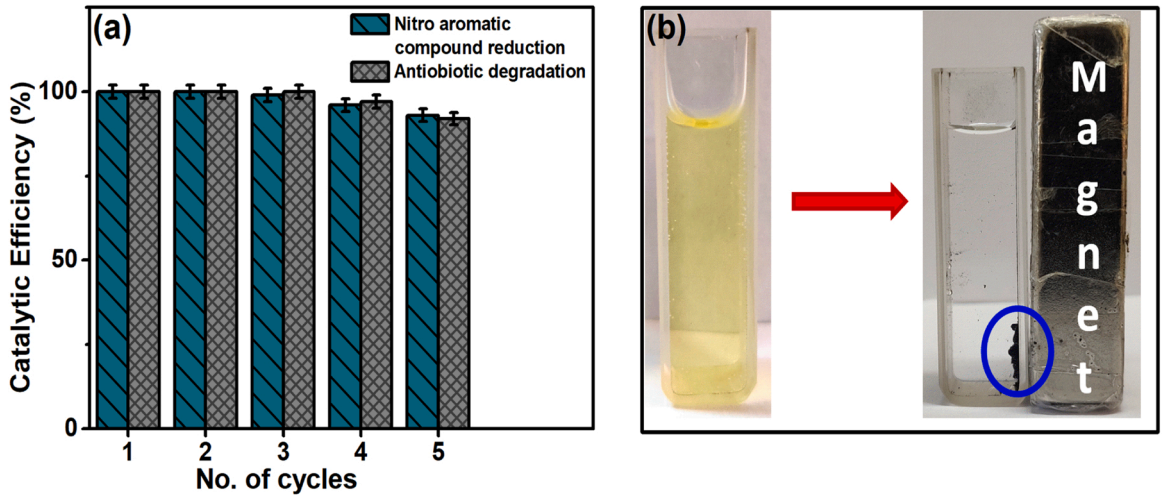

Fig. 10. (a) Reusability of Cu-CF-PC in the reduction of nitroaromatic compounds and antibiotic degradation till 5th cycle, (b) Magnetic separation of the catalyst after completion of the reaction.

of the catalyst slightly decreased (Fig. 10). The structural and morphological stability of Cu-CF-PC after the fifth cycle was investigated by the XRD and FESEM analysis. Fig. S27 displays the XRD pattern and FESEM micrograph of the used catalyst which reveals that there is no significant change in the crystal structure and surface of the catalyst after five consecutive catalysis cycles.

4. Conclusion

In summary, we have successfully synthesized a nanocatalyst Cu-CF-PC and utilized its catalytic efficiency for the removal of water pollutants (aromatic nitrocompounds and antibiotics). Various aromatic nitro compounds were reduced to amine products by the catalyst within 0.5–3 min in the presence of $NaBH_4$, in an aqueous medium, at room temperature. This reaction follows a six-electron transfer route. The catalyst also very efficiently degraded four commonly used antibiotics (AMX, CPX, TCH, and SMX) within 1 min. A Z-scheme heterojunction was induced by microwave irradiation which extends the lifetime of powerful electrons and holes via charge transfer. The intermediates and degraded products were identified by using LC-MS analysis and a plausible degradation scheme was proposed for each of the antibiotics. After completion of the reactions, the catalyst was magnetically recovered from the reaction mixture and was reused. The catalyst exhibited ~92% catalytic efficiency, and no significant change in the crustal structure or morphology was observed even after five cycles. Therefore, Cu-CF-PC can be considered as a promising economically, commercially, and environmentally imperative catalyst which demonstrated its potential usage to overcome the environmental issues related to nitroaromatic compounds and antibiotics.

CRediT authorship contribution statement

Debika Gogoi: Conceptualization, Methodology, Formal analysis, Investigation, Data curation, Writing – original draft, Visualization. **Rajeshvari Samatbhai Karmur:** Formal analysis, Investigation. **Manash R. Das:** XPS analysis, Data curation. **Narendra Nath Ghosh:** Conceptualization, Resources, Writing – review & editing, Supervision.

Declaration of Competing Interest

The authors declare that they have no known competing financial interests or personal relationships that could have appeared to influence the work reported in this paper.

Acknowledgments

Authors want to convey earnest gratitude towards the Central Sophisticated Instrument Facility, BITS Goa for providing XRD, FESEM, Raman facilities, Department of Biological Science and Chemical Engineering, BITS Goa for providing AAS facility and FT-IR facility, Indian Institute of Technology, Hyderabad (IIT-H) for conducting HRTEM, SAED and EDX analysis, and CSIR-North East Institute of Science and Technology, Jorhat for helping with XPS analysis.

Appendix A. Supplementary material

Supplementary data associated with this article can be found in the online version at doi:10.1016/j.apcatb.2022.121407.

References

[1] C. Dey, D. De, M. Nandi, M.M. Goswami, A high performance recyclable magnetic $CuFe_2O_4$ nanocatalyst for facile reduction of 4-nitrophenol, Mater. Chem. Phys. 242 (2020), 122237.
[2] P. Makkar, D. Gogoi, D. Roy, N.N. Ghosh, Dual-purpose $CuFe_2O_4$-rGO-based nanocomposite for asymmetric flexible supercapacitors and catalytic reduction of nitroaromatic derivatives, ACS Omega 6 (2021) 28718–28728.
[3] P. Ding, H. Ji, P. Li, Q. Liu, Y. Wu, M. Guo, Z. Zhou, S. Gao, W. Xu, W. Liu, Visible-light degradation of antibiotics catalyzed by titania/zirconia/graphitic carbon nitride ternary nanocomposites: a combined experimental and theoretical study, Appl. Catal. B 300 (2022), 120633.
[4] T. Aditya, A. Pal, T. Pal, Nitroarene reduction: a trusted model reaction to test nanoparticle catalysts, Chem. Commun. 51 (2015) 9410–9431.
[5] M. Chandel, D. Moitra, P. Makkar, H. Sinha, H.S. Hora, N.N. Ghosh, Synthesis of multifunctional $CuFe_2O_4$-reduced graphene oxide nanocomposite: an efficient magnetically separable catalyst as well as high performance supercapacitor and first-principles calculations of its electronic structures, RSC Adv. 8 (2018) 27725–27739.
[6] J. Feng, L. Su, Y. Ma, C. Ren, Q. Guo, X. Chen, $CuFe_2O_4$ magnetic nanoparticles: a simple and efficient catalyst for the reduction of nitrophenol, Chem. Eng. J. 221 (2013) 16–24.
[7] Y.-T. Zhuang, W. Gao, Y.-L. Yu, J.-H. Wang, Facile fabrication of three-dimensional porous $CuFe_2O_4$ cages as highly efficient and recyclable heterogeneous catalyst, Mater. Des. 130 (2017) 294–301.
[8] M.I. Din, R. Khalid, Z. Hussain, J. Najeeb, A. Sahrif, A. Intisar, E. Ahmed, Critical review on the chemical reduction of nitroaniline, RSC Adv. 10 (2020) 19041–19058.
[9] G. Zhang, F. Tang, X. Wang, P. An, L. Wang, Y.-N. Liu, Co,N-codoped porous carbon-supported CoyZnS with superior activity for nitroarene hydrogenation, ACS Sustain. Chem. Eng. 8 (2020) 6118–6126.
[10] H. Fu, H. Zhang, G. Yang, J. Liu, J. Xu, P. Wang, N. Zhao, L. Zhu, B.H. Chen, Highly dispersed rhodium atoms supported on defect-rich $Co(OH)_2$ for the chemoselective hydrogenation of nitroarenes, New J. Chem. 46 (2022) 1158–1167.
[11] N. Hanna, P. Sun, Q. Sun, X. Li, X. Yang, X. Ji, H. Zou, J. Ottoson, L.E. Nilsson, B. Berglund, Presence of antibiotic residues in various environmental compartments of Shandong province in eastern China: its potential for resistance development and ecological and human risk, Environ. Int. 114 (2018) 131–142.
[12] S.K. Ray, D. Dhakal, S.W. Lee, Insight into sulfamethoxazole degradation, mechanism, and pathways by AgBr-$BaMoO_4$ composite photocatalyst, J. Photochem. Photobiol. A 364 (2018) 686–695.
[13] S. Xin, G. Liu, X. Ma, J. Gong, B. Ma, Q. Yan, Q. Chen, D. Ma, G. Zhang, M. Gao, High efficiency heterogeneous Fenton-like catalyst biochar modified $CuFeO_2$ for the degradation of tetracycline: economical synthesis, catalytic performance and mechanism, Appl. Catal. B 280 (2021), 119386.
[14] X. Si, K. Wu, Y. Si, B. Yousaf, Mechanistic insights into the reactive radicals-assisted degradation of sulfamethoxazole via calcium peroxide activation by manganese-incorporated iron oxide-graphene nanocomposite: Formation of radicals and degradation pathway, Chem. Eng. J. 384 (2020), 123360.
[15] M. Salimi, M. Behbahani, H.R. Sobhi, M. Gholami, A. Jonidi Jafari, R. Rezaei Kalantary, M. Farzadkia, A. Esrafili, A new nano-photocatalyst based on Pt and Bi co-doped TiO_2 for efficient visible-light photo degradation of amoxicillin, New J. Chem. 43 (2019) 1562–1568.
[16] J. Munguia, V. Nizet, Pharmacological targeting of the host-pathogen interaction: alternatives to classical antibiotics to combat drug-resistant superbugs, Trends Pharmacol. Sci. 38 (2017) 473–488.
[17] S. Mishra, P. Kumar, S.K. Samanta, Microwave catalytic degradation of antibiotic molecules by 2D sheets of spinel nickel ferrite, Ind. Eng. Chem. Res. 59 (2020) 15839–15847.
[18] S. Mishra, T.K. Sahu, P. Verma, P. Kumar, S.K. Samanta, Microwave-assisted catalytic degradation of brilliant green by spinel zinc ferrite sheets, ACS Omega 4 (2019) 10411–10418.
[19] D. Gogoi, P. Makkar, N.N. Ghosh, Solar light-irradiated photocatalytic degradation of model dyes and industrial dyes by a magnetic $CoFe_2O_4$-gC_3N_4 S-scheme heterojunction photocatalyst, ACS Omega 6 (2021) 4831–4841.
[20] P. Makkar, A. Malik, N.N. Ghosh, Biomass-derived porous carbon-anchoring $MnFe_2O_4$ hollow sphere and needle-like NiS for a flexible all-solid-state asymmetric supercapacitor, ACS Appl. Energy Mater. 4 (2021) 6015–6024.
[21] D. Gogoi, P. Makkar, M.R. Das, N.N. Ghosh, $CoFe_2O_4$ nanoparticle decorated hierarchical biomass derived porous carbon based nanocomposites for high-performance all-solid-state flexible asymmetric supercapacitor devices, ACS Appl. Electron. Mater. 4 (2022) 795–806.
[22] B.K. Ghosh, S. Hazra, N.N. Ghosh, Synthesis of Cu@CF@SBA15: a Versatile catalysts for (i) reduction of dyes, trifluralin, synthesis of (ii) DHPMs by Biginelli reaction and (iii) 1, 2, 3-triazole derivatives by 'Click reaction', Catal. Commun. 80 (2016) 44–48.
[23] L. Ye, J. Fu, Z. Xu, R. Yuan, Z. Li, Facile one-pot solvothermal method to synthesize sheet-on-sheet reduced graphene oxide (RGO)/$ZnIn_2S_4$ nanocomposites with superior photocatalytic performance, ACS Appl. Mater. Interfaces 6 (2014) 3483–3490.
[24] K.V. Sankar, R.K. Selvan, D. Meyrick, Electrochemical performances of $CoFe_2O_4$ nanoparticles and a rGO based asymmetric supercapacitor, RSC Adv. 5 (2015) 99959–99967.
[25] M. Thommes, K. Kaneko, A.V. Neimark, J.P. Olivier, F. Rodriguez-Reinoso, J. Rouquerol, K.S. Sing, Physisorption of gases, with special reference to the evaluation of surface area and pore size distribution (IUPAC technical report), Pure Appl. Chem. 87 (2015) 1051–1069.
[26] L. Yue, S. Zhang, H. Zhao, Y. Feng, M. Wang, L. An, X. Zhang, J. Mi, One-pot synthesis $CoFe_2O_4$/CNTs composite for asymmetric supercapacitor electrode, Solid State Ion. 329 (2019) 15–24.
[27] S. Sharma, M. Kaur, C. Sharma, A. Choudhary, S. Paul, Biomass-derived activated carbon-supported copper catalyst: an efficient heterogeneous magnetic catalyst for base-free chan–lam coupling and oxidations, ACS Omega 6 (2021) 19529–19545.
[28] L. Hu, M. Li, L. Cheng, B. Jiang, J. Ai, Solvothermal synthesis of octahedral and magnetic $CoFe_2O_4$-reduced graphene oxide hybrids and their photo-Fenton-like behavior under visible-light irradiation, RSC Adv. 11 (2021) 22250–22263.
[29] X.F. Lu, L.F. Gu, J.W. Wang, J.X. Wu, P.Q. Liao, G.R. Li, Bimetal-organic framework derived $CoFe_2O_4$/C porous hybrid nanorod arrays as high-performance electrocatalysts for oxygen evolution reaction, Adv. Mater. 29 (2017), 1604437.
[30] J. Muhommad, L. Kumar, P.K. Baruah, M.R. Das, S. Deka, All-solid-state flexible symmetric supercapacitor based on morphology oriented amorphous Cu-Co-B alloy nanosheets for energy storage, Batter. Supercaps 5 (2022), e202100314.
[31] B. Liu, Y. Liu, H. Chen, M. Yang, H. Li, MnO_2 nanostructures deposited on graphene-like porous carbon nanosheets for high-rate performance and high-energy density asymmetric supercapacitors, ACS Sustain. Chem. Eng. 7 (2019) 3101–3110.
[32] M. Mousavi, A. Habibi-Yangjeh, M. Abitorabi, Fabrication of novel magnetically separable nanocomposites using graphitic carbon nitride, silver phosphate and silver chloride and their applications in photocatalytic removal of different pollutants using visible-light irradiation, J. Colloid Interface Sci. 480 (2016) 218–231.
[33] N. Budhiraja, V. Kumar, S. Singh, Synergistic effect in structural and supercapacitor performance of well dispersed $CoFe_2O_4$/Co_3O_4 nano-hetrostructures, Ceram. Int. 44 (2018) 13806–13814.
[34] C. Lu, Z. Bao, C. Qin, L. Dai, A. Zhu, Facile fabrication of heterostructured cubic-$CuFe_2O_4$/ZnO nanofibers (c-CFZs) with enhanced visible-light photocatalytic activity and magnetic separation, RSC Adv. 6 (2016) 110155–110163.
[35] B. Naik, S. Hazra, D. Desagani, B.K. Ghosh, M.K. Patra, S.R. Vadera, N.N. Ghosh, Preparation of a magnetically separable $CoFe_2O_4$ supported Ag nanocatalyst and its catalytic reaction towards the decolorization of a variety of dyes, RSC Adv. 5 (2015) 40193–40198.
[36] P. Makkar, M. Chandel, M.K. Patra, N.N. Ghosh, A "one-pot" route for the synthesis of snowflake-like Dendritic CoNi alloy-reduced graphene oxide-based multifunctional nanocomposites: an efficient magnetically separable versatile catalyst and electrode material for high-performance supercapacitors, ACS Omega 4 (2019) 20672–20689.
[37] X. Ma, Y.-X. Zhou, H. Liu, Y. Li, H.-L. Jiang, A MOF-derived Co-CoO@N-doped porous carbon for efficient tandem catalysis: dehydrogenation of ammonia borane and hydrogenation of nitro compounds, Chem. Commun. 52 (2016) 7719–7722.
[38] S. Zhang, H. Yin, J. Wang, S. Zhu, Y. Xiong, Catalytic cracking of biomass tar using Ni nanoparticles embedded carbon nanofiber/porous carbon catalysts, Energy 216 (2021), 119285.
[39] S. Padhiari, M. Tripathy, G. Hota, Nitrogen-doped reduced graphene oxide covalently coupled with graphitic carbon nitride/sulfur-doped graphitic carbon nitride heterojunction nanocatalysts for photoreduction and degradation of 4-nitrophenol, ACS Appl. Nano Mater. 4 (2021) 7145–7161.
[40] T.B. Nguyen, C. Huang, R.-A. Doong, Enhanced catalytic reduction of nitrophenols by sodium borohydride over highly recyclable Au@graphitic carbon nitride nanocomposites, Appl. Catal. B 240 (2019) 337–347.
[41] D. Moitra, S. Hazra, B.K. Ghosh, R.K. Jani, M.K. Patra, S.R. Vadera, N.N. Ghosh, A facile low temperature method for the synthesis of $CoFe_2O_4$ nanoparticles possessing excellent microwave absorption properties, RSC Adv. 5 (2015) 51130–51134.
[42] X. Li, Y. Tuo, P. Li, X. Duan, H. Jiang, X. Zhou, Effects of carbon support on microwave-assisted catalytic dehydrogenation of decalin, Carbon 67 (2014) 775–783.
[43] H. Guan, Q. Wang, X. Wu, J. Pang, Z. Jiang, G. Chen, C. Dong, L. Wang, C. Gong, Biomass derived porous carbon (BPC) and their composites as lightweight and efficient microwave absorption materials, Compos. B Eng. 207 (2021), 108562.
[44] J.-B. Cheng, H.-G. Shi, M. Cao, T. Wang, H.-B. Zhao, Y.-Z. Wang, Porous carbon materials for microwave absorption, Mater. Adv. 1 (2020) 2631–2645.

[45] H. Li, H. Yu, X. Quan, S. Chen, Y. Zhang, Uncovering the key role of the fermi level of the electron mediator in a Z-scheme photocatalyst by detecting the charge transfer process of WO_3-metal-gC_3N_4 (Metal= Cu, Ag, Au), ACS Appl. Mater. Interfaces 8 (2016) 2111–2119.
[46] F. Shi, L. Chen, M. Chen, D. Jiang, A gC_3N_4/nanocarbon/$ZnIn_2S_4$ nanocomposite: an artificial Z-scheme visible-light photocatalytic system using nanocarbon as the electron mediator, Chem. Commun. 51 (2015) 17144–17147.
[47] Y. Shiraishi, Y. Ueda, A. Soramoto, S. Hinokuma, T. Hirai, Photocatalytic hydrogen peroxide splitting on metal-free powders assisted by phosphoric acid as a stabilizer, Nat. Commun. 11 (2020) 1–9.
[48] K. Sahel, L. Elsellami, I. Mirali, F. Dappozze, M. Bouhent, C. Guillard, Hydrogen peroxide and photocatalysis, Appl. Catal. B 188 (2016) 106–112.
[49] A.S. Giri, A.K. Golder, Ciprofloxacin degradation from aqueous solution by Fenton oxidation: reaction kinetics and degradation mechanisms, RSC Adv. 4 (2014) 6738–6745.
[50] J. Zia, M. Riyazuddin, E.S. Aazam, U. Riaz, Rapid catalytic degradation of amoxicillin drug using $ZnFe_2O_4$/PCz nanohybrids under microwave irradiation, Mater. Sci. Eng. B 261 (2020), 114713.
[51] Z. Zhang, Z. Pan, Y. Guo, P.K. Wong, X. Zhou, R. Bai, In-situ growth of all-solid Z-scheme heterojunction photocatalyst of $Bi_7O_9I_3$/g-C_3N_4 and high efficient degradation of antibiotic under visible light, Appl. Catal. B 261 (2020), 118212.
[52] P. Mishra, A. Behera, D. Kandi, S. Ratha, K. Parida, Novel magnetic retrievable visible-light-driven ternary Fe_3O_4@$NiFe_2O_4$/phosphorus-doped g-C_3N_4 nanocomposite photocatalyst with significantly enhanced activity through a double-Z-scheme system, Inorg. Chem. 59 (2020) 4255–4272.
[53] T. Ahamad, M. Naushad, S.M. Alshehri, Analysis of degradation pathways and intermediates products for ciprofloxacin using a highly porous photocatalyst, Chem. Eng. J. 417 (2021), 127969.
[54] A. Yazdanbakhsh, A. Eslami, M. Massoudinejad, M. Avazpour, Enhanced degradation of sulfamethoxazole antibiotic from aqueous solution using Mn-WO_3/LED photocatalytic process: kinetic, mechanism, degradation pathway and toxicity reduction, Chem. Eng. J. 380 (2020), 122497.
[55] Y. Zhang, Y. Xiao, Y. Zhong, T.-T. Lim, Comparison of amoxicillin photodegradation in the UV/H_2O_2 and UV/persulfate systems: reaction kinetics, degradation pathways, and antibacterial activity, Chem. Eng. J. 372 (2019) 420–428.
[56] F.T. Joorabi, M. Kamali, S. Sheibani, Effect of aqueous inorganic anions on the photocatalytic activity of CuO-Cu_2O nanocomposite on MB and MO dyes degradation, Mater. Sci. Semicond. Process. 139 (2022), 106335.
[57] J. Wang, B. Xiong, L. Miao, S. Wang, P. Xie, Z. Wang, J. Ma, Applying a novel advanced oxidation process of activated peracetic acid by $CoFe_2O_4$ to efficiently degrade sulfamethoxazole, Appl. Catal. B 280 (2021), 119422.